Optical and electronic properties of doped *p*-type CuI: Explanation of transparent conductivity from first principles

Yuwei Li, Jifeng Sun, and David J. Singh*

Department of Physics and Astronomy, University of Missouri, Columbia, Missouri 65211-7010, USA

(Received 4 January 2018; revised manuscript received 16 February 2018; published 26 March 2018)

We report the properties of the reported transparent conductor CuI, including the effect of heavy *p*-type doping. The results, based on first-principles calculations, include an analysis of the electronic structure and calculations of optical and dielectric properties. We find that the origin of the favorable transparent conducting behavior lies in the absence in the visible of strong interband transitions between deeper valence bands and states at the valence-band maximum that become empty with *p*-type doping. Instead, strong interband transitions to the valence-band maximum are concentrated in the infrared with energies below 1.3 eV. This is contrast to the valence bands of many wide-band-gap materials. Turning to the mobility, we find that the states at the valence-band maximum are relatively dispersive. This originates from their antibonding Cu *d*–I *p* character. We find a modest enhancement of the Born effective charges relative to nominal values, leading to a dielectric constant $\varepsilon(0) = 6.3$. This is sufficiently large to reduce ionized impurity scattering, leading to the expectation that the properties of CuI can still be significantly improved through sample quality.

DOI: 10.1103/PhysRevMaterials.2.035003

I. INTRODUCTION

Transparent conductors (TCs), such as the transparent conducting oxides (TCOs), are compounds that combine low visible light absorption with high electrical conductivity [1,2]. They are important for optoelectronic devices including solar cells and displays, as well as for applications such as smart windows [3–7]. Remarkably, in spite of industrial interest and extensive research, the number of established high-performance TCs suitable for applications is relatively small. These include *n*-type oxides based on In, especially Sn-doped In_2O_3 [8,9], *n*-type stanates including $BaSnO_3$ [10–14], ZnO-based materials [15], and In-Ga-Zn oxides [6].

Good *p*-type TCs are less common, but are enabling for some applications, for example in transparent electronics. However, these *p*-type materials generally have lower performance than state-of-the-art *n*-type TCOs. This fact has motivated several studies of potential *p*-type TCs, leading to the discovery of several new *p*-type TC materials. Known *p*-type TCs include, for example, Cu^+ oxides [16–19], Sn^{2+} compounds [20–23], $BaSnO_3$ [24,25], and Ba_2BiTaO_6 [26].

Recently, CuI has been identified as a good *p*-type TC material [27–32]. CuI has a cubic structure and is also compatible with solar cells and amenable to thin-film growth, including growth on glass [29,33–36]. Here we present a first-principles study of its properties as related to TC behavior, especially the issue of simultaneous conductivity and transparency in a *p*-type material.

We find that a key aspect is the absence of strong interband transitions in the visible when doped, combined with the particular bonding of the material, which favors both *p*-type doping and dispersive valence bands. We do not find strongly enhanced Born effective charges that would lead to unusually high dielectric constants and screening of ionized impurities, in contrast to some other high-mobility halide semiconductors [37,38]. Instead we find a modest enhancement, which nonetheless provides enough screening to suggest that reported *p*-type CuI is not near the limit for increased mobility via sample quality improvements.

II. STRUCTURE AND METHODS

CuI has a zinc-blende structure at temperatures below 643 K (γ phase, space group $F\bar{4}3m$) [39]. The ambient temperature experimental lattice parameter is $a = 6.058$ Å [40], and we used this value. We performed first-principles calculations using the projector augmented-wave (PAW) method [41] as implemented in the VASP code [42] and the general potential linearized augmented-plane-wave (LAPW) [43] method as implemented in the WIEN2K code [44]. We used these two codes because of the ability to apply the virtual crystal approximation and carry out accurate optical calculations provided in WIEN2K and the need to perform hybrid functional and dielectric calculations, which are more convenient in VASP.

We treated the $3d^{10}4s^1$ shells of Cu and the $5s^25p^5$ shells of I as valence electrons with PAW pseudopotentials in our VASP calculations. These were used with kinetic energy cutoffs of 300 eV. We tested to ensure that this was adequate. The *k*-point meshes for sampling the Brillouin zone were at a grid spacing of $2\pi \times 0.02$ Å^{-1} or better, including the hybrid functional calculations. Born effective charges were calculated using density-functional perturbation theory as implemented in VASP. We used sphere radii of 2.46 Bohr for Cu and I and basis-set cutoffs, k_{max}, set by the criterion $R_{min}k_{max} = 9.0$ in the LAPW calculations; here R_{min} is the LAPW sphere radius of 2.46 Bohr. Spin-orbit coupling (SOC) was included

*singhdj@missouri.edu

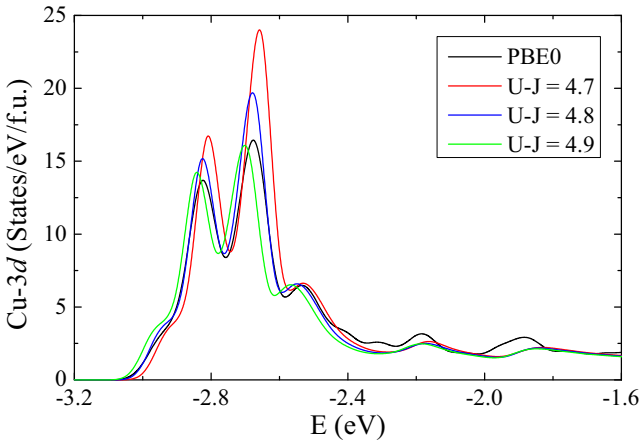

FIG. 1. Calculated valence-band density of states showing the Cu 3*d* states with the PBE0 hybrid functional (black) and GGA+U method when $U = 4.7$ eV (red), 4.8 eV (blue) and 4.9 eV (green). Here J is set to 0 and the energy zero is at the valence-band maximum.

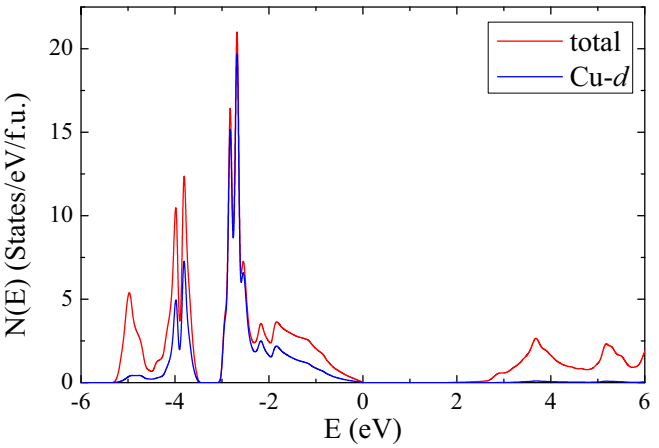

FIG. 2. GGA+U density of states and Cu *d* projection without correction of the band gap.

in all electronic structure and optical property calculations. The spin-orbit calculation was performed in WIEN2K using the second variational approach [43], in which the relativistic problem is solved using a basis set consisting of the scalar relativistic band states. For this purpose, all occupied states plus unoccupied states up to 5 Ry were employed.

Both a correct band gap and a correct position of the Cu *d* states in the I *p* valence bands are important ingredients for obtaining realistic optical and transport properties. We used the generalized gradient approximation (GGA) of Perdew, Burke, and Ernzerhof (PBE) [45], and we applied the GGA+U method to describe the Cu *d* states in LAPW calculations with the WIEN2K code. Transport coefficients were obtained using the BOLTZTRAP code [46]. The value of the parameter U was determined based on hybrid functional calculations with the PBE0 functional [47]. These PBE0 calculations were done using VASP. Good agreement between the PBE0 and GGA+U calculations for the position of the Cu *d* states was obtained for $U = 4.8$ eV, as shown in Fig. 1, which shows the region of the upper crystal-field peak of the Cu *d* density of states. This is the energy range that is crucial for the interband optical absorption in doped *p*-type samples, as discussed below. Importantly, this choice of U in the GGA+U method also yields very good agreement for the shape and peak structure of the Cu *d* density of states. Besides the good agreement between our PBE0 and GGA+U calculations for the shape and position of the Cu *d* states, we note that these are also in good agreement with results from valence-band photoemission experiments [48].

The second issue that is important for optical calculations is the band gap. Calculation of the band gap in CuI is complicated by two issues, namely self-interaction errors associated with the localized Cu *d* electrons, and correct positioning of the Cu *s* derived conduction bands with respect to the I *p* derived valence bands. Because of this combination, the band gap is underestimated even using hybrid functionals and full self-consistent *GW* calculations [49]. This is also the case for our GGA+U calculations, as seen in Fig. 2, which shows the density of states over a wider energy range. Figure 3 shows the relative contribution of the Cu *d* states to the electronic structure. One could in principle shift the band gap by applying fitted U parameters to other orbitals. However, while it is physically clear that there is a need to correct the binding of the localized Cu *d* levels, related to self-interaction errors [50], there is no clear physical basis for applying U parameters to other orbitals in CuI, and in fact the remaining error is more likely associated with the density-functional band-gap underestimation associated with the exchange correlation potential discontinuity [51]. Here we relied on the experimental direct gap (3.1 eV) [52,53], and we applied a rigid shift of the conduction bands to match it.

We then modeled *p*-type CuI using the virtual crystal approximation. The virtual crystal approximation is an average potential approximation. It goes beyond rigid bands and specifically includes composition-dependent distortions of the band structure, although in the present case these distortions are weak. Figure 4 shows the band structure from the hybrid functional calculations, with the shift to reproduce the experimental gap, compared with the virtual crystal band structure at 0.025 holes per formula unit. Optical properties and plasma frequencies were calculated using the optical package

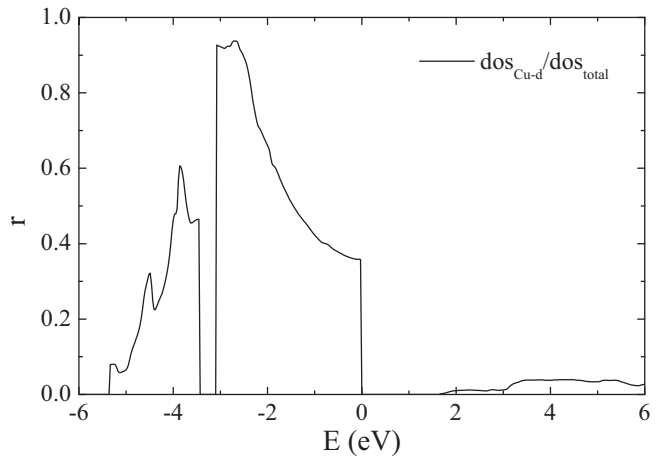

FIG. 3. Ratio of the Cu *d* contribution to the total density of states, as in Fig. 2.

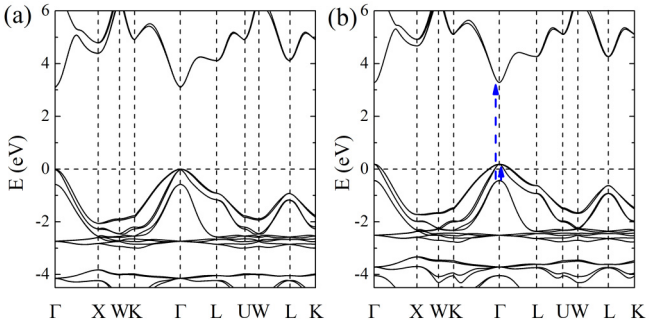

FIG. 4. The valence-band structure of CuI as obtained from hybrid functional calculations (left) and the GGA+U band structure used in the optical and transport calculations (right). Optical transitions are marked with arrows. The solid arrow indicates optical transitions in infrared and the dashed arrow indicates optical transitions in ultraviolet.

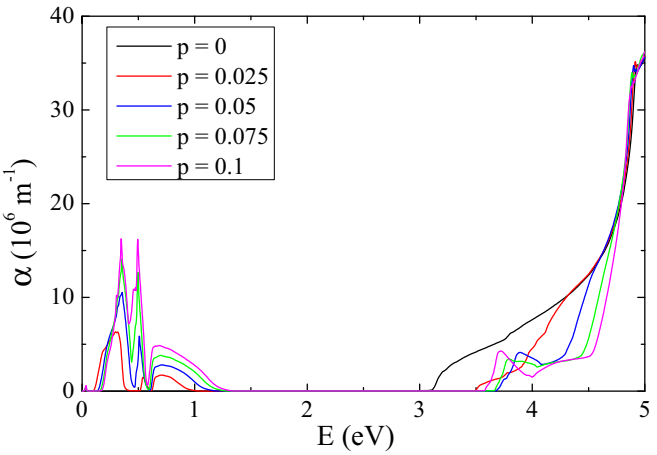

FIG. 5. Calculated absorption coefficient due to interband transitions for p-type CuI as a function of doping level in carriers per Cu atom. In terms of carrier concentration, 0.1 holes per Cu correspond to $p = 1.80 \times 10^{21}$ cm^{-3}. In addition, there will be a Drude part in the infrared with a width that depends on the scattering.

of WIEN2K using virtual crystal band structures obtained for each doping level. In this code, the plasma frequency tensor is calculated as an integral over the Fermi surface of the square band velocity (related to diagonal momentum matrix elements) [54]. We also did rigid band calculations for the transport-related properties using BOLTZTRAP. This calculation differs from the plasma frequency calculation in that it does not include distortions of the band structure from changes in the electron count. These distortions are included in the virtual crystal approximation, but not in the rigid band approximation. Furthermore BOLTZTRAP uses an analytic expression for the band velocity based on a very fine grid Fourier interpolation of the energy eigenvalues, different from the optical package of WIEN2K. We find that for CuI the rigid transport calculations yield similar results to the virtual crystal approximation for the plasma frequency.

III. RESULTS AND DISCUSSION

The band structure (Fig. 4, shown for 0.025 holes per Cu, i.e., $p = 4.5 \times 10^{20}$ cm^{-3} in the right panel) illustrates one of the main conundrums in TC materials: a TC must be both transparent and conducting at the same time under the same conditions. The band gap of CuI, as is known from experiment, is 3.1 eV, meaning that intrinsic CuI of sufficient quality should be transparent for almost all of the visible spectrum. It is also known from experiment and expected from the chemistry of compounds of monovalent Cu that the compound naturally forms p-type and can be relatively easily p-type doped, and then becomes conducting. The band structure shows dispersive bands at the valence-band maximum (quantified below in terms of a transport effective mass) consistent with reasonable conduction.

The dispersive nature of the bands arises because, as seen in the density of states, they have antibonding Cu d–I p character, similar to other d^{10} semiconductors [55]. This is clearly seen in the density of states, and in particular the Cu d contribution (Fig. 3). The antibonding I p–Cu d nature of the states at the top of the valence band causes them to be higher in energy than a pure I p valence band would be, leading to increased dispersion, as has been discussed in other compounds [55].

The problem is that conduction requires doping. CuI, like many materials, shows several bands near the valence-band maximum, including the energy range from −3.25 to −1.65 eV, which corresponds to the visible. p-type doping introduces empty states at the valence-band maximum, and then one may anticipate transitions from the deeper bands to the empty states, with associated absorption of visible light. In known high-performance n-type TCOs, e.g., In_2O_3, $BaSnO_3$, and ZnO, there are no conduction bands with energies that would allow direct transitions in the visible from the conduction-band minimum [56–58]. Thus, while undoped CuI is expected to be transparent due to the band gap, and doped CuI is expected to conduct due to the dispersion of the bands at the valence-band maximum, it may at first glance be unclear how doped CuI can retain transparency.

We begin with the optical properties of p-type CuI, based on virtual crystal calculations that explicitly include doping-induced empty states at the top of the valence bands and transitions into these states. Figure 5 shows the absorption spectra for different p-type doping levels based on interband transitions. For zero doping there is a strong absorption edge at the direct band gap due to dipole-allowed transitions from the valence-band maximum to the conduction-band minimum. These transitions are removed by p-type doping as the initial states become unoccupied. This is basically a Burstein-Moss shift. The strong absorption feature above the gap comes from the second split-off hole band for heavily doped material, as shown, while additional strong absorption in the infrared appears from interband transitions within the valence bands. In addition to the interband transitions, there will be a Drude component, which depends on the doping-dependent plasma frequency (see below) and the usually sample-dependent scattering rate. This will yield additional infrared absorption, which we do not include.

As mentioned, undoped CuI is a semiconductor with a direct band gap and onset of absorption at >3.1 eV. Doping introduces additional strong absorption peaks in the infrared

(<1.3 eV) due to interband transitions. This is in contrast to many n-type TCOs, such as ITO, ZnO, and $BaSnO_3$, and reflects the availability of valence bands to participate in transitions to empty states at the valence-band maximum. Thus, p-type CuI is not transparent for infrared light.

The key present finding of our study as regards optical properties is that there are no significant interband transitions in the visible part of the spectrum for p-type CuI. The origin is in the gap at Γ between the upper d crystal-field level and the valence-band maximum, as well as weak matrix elements between the d states and the top valence band near Γ (note that the symmetry of the fourfold-degenerate state at the valence-band maximum is the same as the top Cu d band at Γ). This is qualitatively similar to what was recently found for another recently discovered p-type TCO, $K_xBa_{1-x}SnO_3$ [24,25]. The TC behavior of p-type CuI depends on this feature of its band structure.

Figure 4 shows the band structure with p-type CuI, comparing the hybrid functional and PBE+U calculations (both with the conduction-band shift to reproduce the experimental band gap). The virtual crystal band structure shown in the right panel is at a carrier concentration of 0.025 holes per Cu ($p = 4.5 \times 10^{20}$ cm^{-3}). The solid vertical arrow in the band-structure plot indicates the main transitions in the infrared, which are between bands below the valence-band maximum and the top band. The dashed arrow indicates the transition between valence bands and conduction bands with energy >3.5 eV, as seen in Fig. 5.

The valence-band maximum at Γ is fourfold-degenerate (including spin), as is common to most zinc-blende semiconductors. The fact that I ($Z = 53$) is a heavy p-electron element, combined with the fact that the crystal structure is noncentrosymmetric, with significantly different atoms on the two sites (Cu and I), results in tiny but non-negligible spin-orbit splittings of these bands as one moves away from Γ, so that the top four bands are formally distinct, though neglecting these spin splittings away from Γ they are simply the heavy-hole and light-hole band characteristic of zinc-blende semiconductors such as GaAs.

There is an additional hole band starting ∼0.6 eV below the valence-band maximum. This twofold-degenerate (including spin) band is split from the valence-band maximum by spin orbit. It is similar to the corresponding band in GaAs, but the splitting is larger due to the higher atomic number of I, relative to As. The splitting of 0.6 eV is comparable to that found in GaSb (∼0.7 eV), containing Sb ($Z = 51$) [59,60]. This band ordering is in accord with experimental data [59,61]. Importantly, transitions from this lower split-off band to the valence-band maximum are dipole-allowed in the noncentrosymmetric zinc-blende structure. The symmetry breaking from diamond structure is strong in CuI because of the very different chemical natures of Cu and I.

The other key property of a good TC is high conductivity. In practice, doping is essential for increasing the conductivity of TCO thin films, but usually heavy carrier concentration reduces the transparency. Experimentally, in samples produced so far, the transmittance of CuI is reported to reach 72% at a conductivity level of 280 S cm^{-1} [27]. Here we use the quantity σ/τ (σ is conductivity and τ is an effective scattering time) to characterize the transport properties of p-type CuI. This

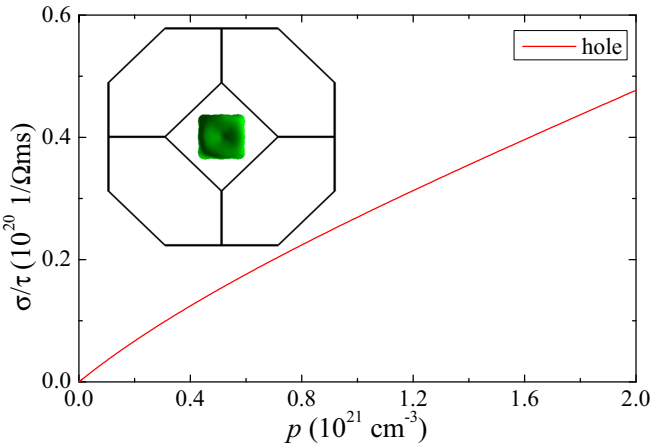

FIG. 6. σ/τ of p-type CuI (red) as a function of carrier concentration as obtained at 300 K. The inset is the energy isosurface for 0.025 holes per Cu, as shown in Fig. 4. This corresponds to a carrier concentration, $p = 4.5 \times 10^{20}$ cm^{-3}.

quantity is calculated directly from the band structure using the linearized Boltzmann transport theory with the relaxation-time approximation, as implemented in the BoltzTraP code. Figure 6 shows this quantity as a function of doping level, based on the rigid band approximation as determined using the BoltzTraP code. As seen, σ/τ increases roughly linearly with carrier concentration (characteristic behavior of a parabolic band semiconductor) at low carrier concentration. In comparing different materials, it is conventional to map the properties onto a single parabolic band model, even in cases such as CuI, where there are multiple bands at the valence-band maximum. This allows, for example, comparison of an effective mass between different compounds, with low effective mass indicating the likelihood of good mobility and conductivity when doped [26]. Matching the calculated σ/τ to a single parabolic band model, we obtain a transport effective mass of $m_h = 0.77m_e$ (m_e is the mass of the electron) for carrier concentrations p up to the 10^{19} cm^{-3} level, and then increasing weakly to $1.05m_e$ for $p = 10^{21}$ cm^{-3}. This carrier concentration dependence shows the nonparabolicity of the bands. Nonparabolicity with increasing mass away from Γ-point valence-band maxima, especially for the light-hole band, is a characteristic of zinc-blende semiconductors consistent with what we find, e.g., along Γ-L [62].

As mentioned, while it is useful to compare materials based on a transport effective mass, the valence band structure of γ-CuI does not show a single parabolic band at the band edge, and even considering a two-band model with a light- and heavy-hole band, one may see substantial nonparabolicity. We show the isoenergy surface of the top band for a p-type doping of 0.025 holes per Cu in the inset of Fig. 6. Carrier pockets for the top four bands, comprising the spin-orbit-split heavy- and light-hole bands, are shown for different Fermi levels in Fig. 7. For isolated noninteracting parabolic bands with cubic symmetry, these would be simple spheres. Clearly the shapes deviate strongly from spheres, particularly for the heavy-hole bands. This is a consequence of the momentum-dependent splitting of the bands at the valence-band maximum as one moves away from the Γ point. The result of this type of

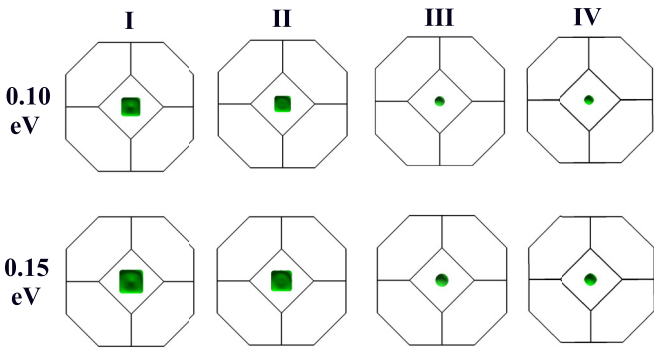

FIG. 7. Isosurfaces of the four top bands comprising the spin-orbit-split heavy- and light-hole bands for different Fermi energies as shown.

complexity is generally a decoupling of the transport and density-of-states effective masses in a way that lowers the transport effective mass, and is therefore favorable for the mobility [63,64]. It should also be noted that the two light-hole bands have more spherical isosurfaces. The average mass of these two light-hole bands is $0.25m_e$, and actually varies between $0.23m_e$ and $0.28m_e$, depending on direction, again reflecting the anisotropy of the carrier pockets.

The calculated 0 K plasma frequencies, $\Omega_p = \hbar\omega_p$, as a function of doping level, are given in Fig. 8 along with those of $CuAlO_2$ and Cu_2O. These were obtained using the virtual crystal approximation, done by lowering the atomic number of Cu to model p-type doping due to Cu vacancies, known to be important sources of p-type conduction in those materials. Conductivity in metals and degenerately doped semiconductors depends on the plasma frequency, $\sigma \propto \Omega_p^2\tau$, where τ is an effective inverse scattering rate (at 0 K, $\varepsilon_0\omega_p = \sigma/\tau$). As shown in Fig. 8, the plasma frequency for CuI is significantly higher than $CuAlO_2$, consistent with good TC performance, and perhaps better performance than $CuAlO_2$ depending on the scattering rate. It is also important to note that the doping dependence of the virtual crystal plasma frequency and that of

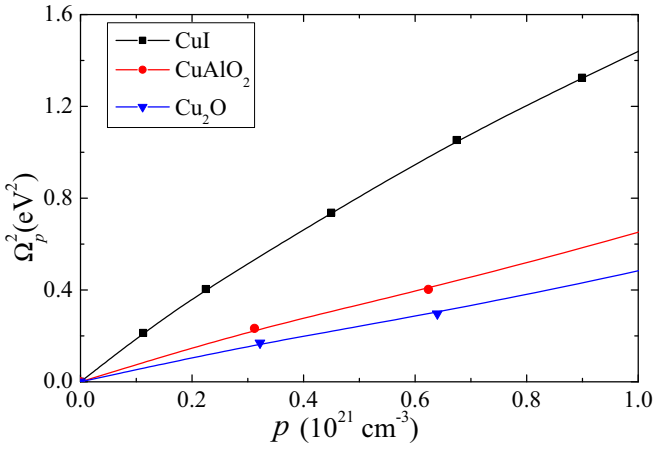

FIG. 8. Squared plasma frequency of p-type CuI (black), $CuAlO_2$ (red), and Cu_2O (blue) as a function of carrier concentration, as obtained from virtual crystal calculations for $Cu_{1-x}I$ and for $CuAlO_2$ and Cu_2O with virtual crystal p-type doping on the O site.

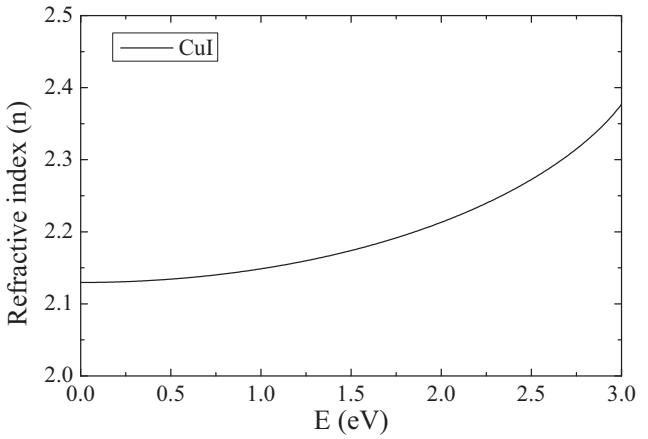

FIG. 9. Calculated refractive index as a function of energy.

rigid band σ/τ for CuI are very similar, supporting *a posteriori* the use of these approximations.

The reported experimental temperature-dependent resistivity of heavily p-type degenerate doped CuI is consistent with a resistivity that is dominated by defect scattering, especially ionized impurity scattering and grain boundary scattering rather than electron-phonon scattering [27]. As such, the question arises as to the extent to which the scattering can be improved, e.g., by improvements in sample quality. Some level of ionized impurity scattering is inevitable in heavily doped bulk semiconductors as a result of the dopants. This sets an upper limit on the conductivity. This limit is very sensitive to the dielectric constant [65,66]. In the case in which only ionized impurity scattering applies, the mobility, μ, varies as the square of the static zero-frequency dielectric constant [67].

Our optical calculations without doping and including only the electronic response yield a low-frequency refractive index, $n(0) = 2.13$, which is in good agreement with literature values, $n(0) = 2.14$ (Ref. [68]) and $n(0) = 2.20$ (Ref. [69]). The energy dependence is shown in Fig. 9. Our low-energy value corresponds to an optical dielectric constant, $\varepsilon(\infty) = 4.53$.

Ionized impurity scattering is, however, governed by the static dielectric constant, including the lattice and electronic parts. Experimentally, CuI is invariably a p-type doped semiconductor due to the presence of Cu vacancies. The resulting conductivity complicates measurements of the static dielectric constant. Literature values range from $\varepsilon(0) = 6.5$ to $\varepsilon(0) = 15$ [68,70,71]. In addition, it should be noted that the cuprous halides, including CuI, are near a structural phase transition, reflecting borderline stability of the zinc-blende structure against a more ionic rock structure, as is seen in the pressure-dependent phase transitions and in plots of structure versus Phillips ionicity. This leads to anomalous lattice dynamics, affecting the validity of the Lynddane-Sachs-Teller relation that may otherwise be used to estimate $\varepsilon(0)$ from phonon measurements as well as properties such as thermal conductivity [72–75].

We calculated the lattice part of the dielectric constant and the Born charges with the PBE GGA using VASP. We also calculated the electronic dielectric constant in the same way. The electronic dielectric constant from these PBE GGA calculations was 4.77, slightly larger than from the PBE+U calculations with WIEN2K as might be anticipated in view of the

lower band gap in the PBE GGA calculations. The difference between the PBE GGA and the PBE+U calculations of the electronic dielectric constant with WIEN2K (including for the PBE+U calculation the shift of the conduction bands to match the experimental gap) amounts to ∼5%, which implies that the effect of the density-functional band-gap error on the electronic dielectric constant is relatively small in CuI.

The electronic-structure results show a near-ionic situation, with occupied I p bands, and states near the conduction-band minimum having Cu s character. As such, one may write a nominally ionic model, Cu^+I^-, with nominal charges ±1 on the two ions. We obtained calculated Born charges $Z^* = \pm 1.10$, i.e., weakly enhanced from these nominal values of ±1. Such an enhancement in the zinc-blende structure is unusual, and presumably reflects the significant ionicity of the compound combined with cross-gap hybridization between the I p derived orbitals in the valence bands and the Cu states in the conduction bands, consistent with a recent discussion of the bonding based on first-principles calculations [49]. However, the enhancement of the Born charges in CuI is not large enough to lead to a large enhancement of the dielectric constant. Our calculated value is $\varepsilon(0) = 6.3$, which is at the lower end of the literature experimental values, supporting the direct low-temperature electrical measurements of Hanson and co-workers [70]. It should be noted, however, that while smaller than the dielectric constant of high-performance halide semiconductors, such as TlBr or the Pb halide perovskite solar absorbers [37,38], it is still sufficient that the limit on the mobility due to ionized impurity scattering is well below reported values. For example, Grundmanm and co-workers [29] report a mobility fit to the Shockley expression for a degenerate semiconductor, and they obtain a constant of $\sim 0.25 c_s$. Here c_s is the coefficient for the scattering rate for electrons of mass m_e with dielectric constant unity. Within such models, the scattering rate is proportional to the mass and inversely proportional to the square of the dielectric constant. Our dielectric constant of ∼6 would leave room for a very substantial improvement. While this is a very crude estimate and it ignores other sources of scattering, including the unavoidable electron-phonon scattering, it does still imply that substantial improvement in the mobility remains possible from improvement in sample quality. Furthermore, we note that the relatively modest dielectric constant of CuI suggests that there may be room for improving the electrical properties by, for example, alloying as in other cases [55]. Alloying to increase the value of $\varepsilon(0)$ has been discussed and was shown experimentally to be effective for another material [65]. We do, however, note that alloying involves alloy scattering and increased possibilities for defects, which may work against the mobility.

IV. SUMMARY AND CONCLUSIONS

We present first-principles calculations of optical and electronic properties of p-type CuI, explaining the nature of its high transparency and conductivity. The calculations show that although p-type doping of CuI produces strong optical absorption in the infrared below 1.3 eV, high transparency in the visible is retained due to the specific band structure. We also find a band structure consistent with reasonable conduction based on the calculated transport functions. The high visible transparency of doped CuI is a characteristic that depends on the details of the electronic structure, and it goes beyond the oft-quoted requirements of low effective mass and sufficient band gap for transparent conductors. In addition, we find a dielectric constant that, while smaller than other high-performance halide semiconductors, is nonetheless large enough to imply that the mobility of CuI samples reported in the literature can still be substantially improved by improvements in sample quality.

ACKNOWLEDGMENTS

This work was supported by the Department of Energy through the S3TEC Energy Frontier Research Center, Award No. DE-SC0001299/DE-FG02ER46577.

[1] K. Chopra, S. Major, and D. Pandya, Thin Solid Films **102**, 1 (1983).
[2] A. Stadler, Materials (Basel) **5**, 661 (2012).
[3] D. S. Ginley and C. Bright, MRS Bull. **25**, 15 (2000).
[4] H. Kawazoe, H. Yanagi, K. Ueda, and H. Hosono, MRS Bull. **25**, 28 (2000).
[5] F. N. Ishikawa, H.-K. Chang, K. Ryu, P.-C. Chen, A. Badmaev, L. Gomez De Arco, G. Shen, and C. Zhou, ACS Nano **3**, 73 (2009).
[6] K. Nomura, H. Ohta, A. Takagi, T. Kamiya, M. Hirano, and H. Hosono, Nature (London) **432**, 488 (2004).
[7] H. Q. Chiang, J. F. Wager, R. L. Hoffman, J. Jeong, and D. A. Keszler, Appl. Phys. Lett. **86**, 013503 (2005).
[8] H. L. Hartnagel, A. L. Dawar, A. K. Jain, and C. Jagadish, *Semiconducting Transparent Thin Films* (Institute of Physics, Bristol, 1995).
[9] T. Minami, Thin Solid Films **516**, 5822 (2008).
[10] H. F. Wang, Q. Z. Liu, G. Y. Gao, and W. Wu, J. Appl. Phys. **101**, 106105 (2007).
[11] S. Sallis, D. O. Scanlon, S. C. Chae, N. F. Quackenbush, D. A. Fischer, J. C. Woicik, J. H. Guo, S. W. Cheong, and L. F. J. Piper, Appl. Phys. Lett. **103**, 042105 (2013).
[12] H. Mizoguchi, P. Chen, P. Boolchand, V. Ksenofontov, C. Felser, P. W. Barnes, and P. M. Woodward, Chem. Mater. **25**, 3858 (2013).
[13] D. J. Singh, Q. Xu, and K. P. Ong, Appl. Phys. Lett. **104**, 011910 (2014).
[14] Y. Li, L. Zhang, Y. Ma, and D. J. Singh, APL Mater. **3**, 011102 (2015).
[15] D. G. Thomas, J. Phys. Chem. Solids **15**, 86 (1960).
[16] H. Kawazoe, M. Yasukawa, H. Hyodo, M. Kurita, H. Yanagi, and H. Hosono, Nature (London) **389**, 939 (1997).
[17] N. Duan, A. W. Sleight, M. K. Jayaraj, and J. Tate, Appl. Phys. Lett. **77**, 1325 (2000).

[18] K. Ueda, S. Inoue, S. Hirose, H. Kawazoe, and H. Hosono, Appl. Phys. Lett. **77**, 2701 (2000).
[19] R. Nagarajan, A. D. Draeseke, A. W. Sleight, and J. Tate, J. Appl. Phys. **89**, 8022 (2001).
[20] Y. Li, D. J. Singh, M.-H. Du, Q. Xu, L. Zhang, W. Zheng, and Y. Ma, J. Mater. Chem. C **4**, 4592 (2016).
[21] A. Behrendt, C. Friedenberger, T. Gahlmann, S. Trost, T. Becker, K. Zilberberg, A. Polywka, P. Görrn, and T. Riedl, Adv. Mater. **27**, 5961 (2015).
[22] E. Fortunato, R. Barros, P. Barquinha, V. Figueiredo, S.-H. K. Park, C.-S. Hwang, and R. Martins, Appl. Phys. Lett. **97**, 052105 (2010).
[23] J. A. Caraveo-Frescas, P. K. Nayak, H. A. Al-Jawhari, D. B. Granato, U. Schwingenschlögl, and H. N. Alshareef, ACS Nano **7**, 5160 (2013).
[24] H. M. Kim, U. Kim, C. Park, H. Kwon, and K. Char, APL Mater. **4**, 056105 (2016).
[25] Y. Li, J. Sun, and D. J. Singh, Appl. Phys. Lett. **110**, 051904 (2017).
[26] A. Bhatia, G. Hautier, T. Nilgianskul, A. Miglio, J. Sun, H. J. Kim, K. H. Kim, S. Chen, G.-M. Rignanese, X. Gonze, and J. Suntivich, Chem. Mater. **28**, 30 (2015).
[27] C. Yang, M. Kneiss, M. Lorenz, and M. Grundmann, Proc. Natl. Acad. Sci. USA **113**, 12929 (2016).
[28] C. Yang, D. Souchay, M. Kneiß, M. Bogner, H. Wei, M. Lorenz, O. Oeckler, G. Benstetter, Y. Q. Fu, and M. Grundmann, Nat. Commun. **8**, 16076 (2017).
[29] M. Grundmann, F.-L. Schein, M. Lorenz, T. Böntgen, J. Lenzner, and H. von Wenckstern, Phys. Status Solidi A **210**, 1671 (2013).
[30] J. Wang, J. Li, and S.-S. Li, J. Appl. Phys. **110**, 054907 (2011).
[31] D. Chen, Y. Wang, Z. Lin, J. Huang, X. Chen, D. Pan, and F. Huang, Cryst. Growth Des. **10**, 2057 (2010).
[32] F.-L. Schein, H. von Wenckstern, and M. Grundmann, Appl. Phys. Lett. **102**, 092109 (2013).
[33] J.-H. Lee, D.-S. Leem, and J.-J. Kim, Org. Electron. **9**, 805 (2008).
[34] Y. Zhou, T. Taima, T. Miyadera, T. Yamanari, M. Kitamura, K. Nakatsu, and Y. Yoshida, Nano Lett. **12**, 4146 (2012).
[35] C. Yang, M. Kneiß, F.-L. Schein, M. Lorenz, and M. Grundmann, Sci. Rep. **6**, 21937 (2016).
[36] B. L. Zhu and X. Z. Zhao, Phys. Status Solidi A **208**, 91 (2011).
[37] M.-H. Du and D. J. Singh, Phys. Rev. B **81**, 144114 (2010).
[38] W. Ming, H. Shi, and M. H. Du, J. Mater. Chem. A **4**, 13852 (2016).
[39] D. A. Keen and S. Hull, J. Phys.: Condens. Matter **7**, 5793 (1995).
[40] C. D. Carpentier and R. Nitsche, Mater. Res. Bull. **9**, 1097 (1974).
[41] G. Kresse and D. Joubert, Phys. Rev. B **59**, 1758 (1999).
[42] G. Kresse and J. Furthmüller, Phys. Rev. B **54**, 11169 (1996).
[43] D. J. Singh and L. Nordstrom, *Planewaves, Pseudopotentials, and the LAPW Method*, 2nd ed. (Springer, Berlin, 2006).
[44] P. Blaha, K. Schwarz, G. K. H. Madsen, D. Kvasnicka, and J. Luitz, WIEN2K, An augmented plane wave+ local orbitals program for calculating crystal properties (2001).
[45] J. P. Perdew, K. Burke, and M. Ernzerhof, Phys. Rev. Lett. **77**, 3865 (1996).
[46] G. K. H. Madsen and D. J. Singh, Comput. Phys. Commun. **175**, 67 (2006).
[47] C. Adamo and V. Barone, J. Chem. Phys. **110**, 6158 (1999).
[48] A. V. Generalov and A. S. Vinogradov, Phys. Solid State **55**, 1136 (2013).
[49] A. Pishtshev and S. Z. Karazhanov, J. Chem. Phys. **146**, 064706 (2017).
[50] J. P. Perdew and A. Zunger, Phys. Rev. B **23**, 5048 (1981).
[51] J. P. Perdew and M. Levy, Phys. Rev. Lett. **51**, 1884 (1983).
[52] K. Tennakone, G. R. R. A. Kumara, I. R. M. Kottegoda, V. P. S. Perera, G. M. L. P. Aponsu, and K. G. U. Wijayantha, Sol. Energy Mater. Sol. Cells **55**, 283 (1998).
[53] S. E. Derenzo, M. J. Weber, and M. K. Klintenberg, Nucl. Instrum. Methods Phys. Res., Sect. A **486**, 214 (2002).
[54] C. Ambrosch-Draxl and J. O. Sofo, Comput. Phys. Commun. **175**, 1 (2006).
[55] B. A. D. Williamson, J. Buckeridge, J. Brown, S. Ansbro, R. G. Palgrave, and D. O. Scanlon, Chem. Mater. **29**, 2402 (2017).
[56] O. N. Mryasov and A. J. Freeman, Phys. Rev. B **64**, 233111 (2001).
[57] D. J. Singh, D. A. Papaconstantopoulos, J. P. Julien, and F. Cyrot-Lackmann, Phys. Rev. B **44**, 9519 (1991).
[58] A. Janotti and C. G. Van de Walle, Rep. Prog. Phys. **72**, 126501 (2009).
[59] P. D. O. Madelung, *Semiconductors: Data Handbook* (Springer, Berlin, 2004).
[60] M. Gmitra and J. Fabian, Phys. Rev. B **94**, 165202 (2016).
[61] A. Goldmann, Phys. Status Solidi B **81**, 9 (1977).
[62] E. O. Kane, J. Phys. Chem. Solids **1**, 249 (1957).
[63] N. A. Mecholsky, L. Resca, I. L. Pegg, and M. Fornari, Phys. Rev. B **89**, 155131 (2014).
[64] G. Xing, J. Sun, Y. Li, X. Fan, W. Zheng, and D. J. Singh, Phys. Rev. Mater. **1**, 065405 (2017).
[65] J. Shuai, J. Mao, S. Song, Q. Zhu, J. Sun, Y. Wang, R. He, J. Zhou, G. Chen, D. J. Singh, and Z. Ren, Energy Environ. Sci. **10**, 799 (2017).
[66] J. Sun and D. J. Singh, Phys. Rev. Appl. **7**, 024015 (2017).
[67] P. Debye and E. Conwell, Phys. Rev. **93**, 693 (1954).
[68] L. A. Ageev, V. K. Miloslavskii, and T. I. Maksimenko, Opt. Spectrosc. (USSR) **36**, 76 (1974).
[69] J. E. Potts, R. C. Hanson, C. T. Walker, and C. Schwab, Solid State Commun. **13**, 389 (1973).
[70] R. C. Hanson, J. R. Hallberg, and C. Schwab, Appl. Phys. Lett. **21**, 490 (1972).
[71] J. N. Plendl, A. Hadni, J. Claudel, Y. Henninger, G. Morlot, P. Strimer, and L. C. Mansur, Appl. Opt. **5**, 397 (1966).
[72] R. M. Martin, Phys. Rev. B **1**, 4005 (1970).
[73] B. Hennion, F. Moussa, B. Prevot, C. Carabatos, and C. Schawb, Phys. Rev. Lett. **28**, 964 (1972).
[74] C. H. Park and D. J. Chadi, Phys. Rev. Lett. **76**, 2314 (1996).
[75] S. Mukhopadhyay, D. Bansal, O. Delaire, D. Perrodin, E. Bourret-Courchesne, D. J. Singh, and L. Lindsay, Phys. Rev. B **96**, 100301 (2017).